Hollow Fiber Nanofiltration Membranes with Integrated Aquaporin Z

Journal:	*New Journal of Chemistry*
Manuscript ID	NJ-ART-08-2018-004367.R1
Article Type:	Paper
Date Submitted by the Author:	01-Oct-2018

Complete List of Authors:	Sengur-Tasdemir, Reyhan; Istanbul Technical University, Nanoscience and Nanoengineering; Istanbul Technical University, National Research Center on Membrane Technologies sayinli, burcu; Istanbul Technical University, Nanoscience and Nanoengineering Urper, Gulsum; Istanbul Techincal University, Environmental Engineering Tutuncu, Esra; Istanbul Technical University, Molecular Biology and Genetics Karaguler, Nevin ; Istanbul Teknik Universitesi Fen Bilimleri Enstitusu, Molecular Biology and Genetics Ates-Genceli, Esra; Istanbul Technical University, Environmental Engineering Tarabara, Volodymyr; Michigan State University, Civil and Environmental Engineering Koyuncu, Ismail; Istanbul Technical University, Department of Environmental Engineering

Hollow Fiber Nanofiltration Membranes with Integrated Aquaporin Z

Reyhan Sengur-Tasdemir[1,2], Burcu Sayinli[1,2], Gulsum Melike Urper[2,3], Esra Tutuncu[4], Nevin Gul Karaguler[4], Esra Genceli[2,3], Volodymyr V. Tarabara[5], Ismail Koyuncu[1,2,3,*]

[1] Nanoscience and Nanoengineering Department, Istanbul Technical University, 34469, Istanbul, Turkey
[2] National Research Center on Membrane Technologies, Istanbul Technical University, 34469, Istanbul, Turkey
[3] Environmental Engineering Department, Istanbul Technical University, 34469, Istanbul, Turkey
[4] Molecular Biology and Genetics Department, Istanbul Technical University, 34469, Istanbul, Turkey
[5] Department of Civil and Environmental Engineering, Michigan State University, East Lansing, MI 48824, USA

Abstract

We report on the preparation of hollow fiber nanofiltration membranes with Aquaporin Z immobilized on the outer surface of the separation layer. Three ultrafiltration supports – polymeric, nanocomposite and reinforced were evaluated in terms of their effect on the separation properties of membranes with AqpZ. Surface characterization showed that AqpZ-reconstituted proteoliposomes were successfully integrated with the polyamide matrix leading to permeate flux enhancement of up to 2.5 times. The membranes were also evaluated in terms of salt and organic matter removal. Reinforced ultrafiltration support allowed for the most effective integration between the polyamide layer and proteoliposomes giving the highest figure of merit – an aggregate metric of membrane performance that includes water permeability, selectivity and resistance to fouling.

Keywords: Aquaporin z, hollow fiber membrane, nanofiltration, polyamide, reinforced support

1. Introduction

Continued progress in water treatment technologies is driven by the global water demand and increasingly stringent water quality standards. High quality water can be produced using synthetic membranes. Within the family of membrane technologies, nanofiltration (NF) occupies an important niche due to the combination of relatively low operating pressures and ability to remove large ions and natural organic matter [1, 2]. Novel membrane materials such as Aquaporin, can further reduce the energy cost requirements of NF [3]. As an intrinsic membrane protein, Aquaporin enables high water flux due to the formation of specific hydrogen bonds between the protein's water transport channel and water molecules. In addition, aquaporin features high selectivity due to desolvation effects and size exclusion by the narrowest part of the pore, which rejects hydrated ions larger than the pore [4, 5]. A single aquaporin can transfer up to $8 \cdot 10^9$ water molecules per second which equals to 0.86 picoliters per hour. The permeability of one of the first membranes with AqpZ was reported to be 167 $(\mu m/s)bar^{-1}$(601 LMH/bar), which compared very favorably with permeabilities of commercial forward osmosis (FO) and reverse osmosis (RO) membranes: 0.22 $(\mu m/s)bar^{-1}$ (0.8 LMH/bar) and 2 $(\mu m/s)bar^{-1}$,(7.2 LMH/bar), respectively [3].

Within eleven years of the publication of the first paper on the use of Aquaporin Z (AqpZ) as a component of a synthetic membrane [3], several literature reviews [5-10] and many research papers have appeared on the design of AqpZ-enabled membranes [11-19]. Design approaches explored in these studies fall into two groups, which can be classified as based on planar [16, 20-23] and vesicular strategies [14, 15, 17-19]. In the former group, vesicles with AqpZ are directly fused onto the dense separation layer of a membrane; such membranes, however, suffer from defects, unsuccessful reconstitution of AqpZ, and scale-up challenges. The more recent vesicular methods are based on the incorporation of AqpZ-containing vesicles onto the membrane surface by polymerization, self-assembly with polyelectrolytes, or by crosslinking. Li et al. [24]

suggested that coating of polymerized layers, crosslinking and self-assembly have higher potential to reduce defect formation compared to the planar methods.

Although studies exist for commercial AqpZ inside FO hollow fiber (HF) membrane applications [25, 26], regarding the fabrication of AqpZ immobilized membranes, almost all published studies were performed using flat sheet membranes. To our knowledge, there have been only two studies with AqpZ as a component of hollow fiber membranes. In both studies, AqpZ immobilized inside of hollow fiber membranes. Li et al. immobilized AqpZ-containing vesicles onto the inner surface of hollow fiber membranes by interfacial polymerization using m-phenylene diamine (MPD) and trimesoyl chloride (TMC) as monomers for RO and FO applications [24]; as a result of the modification, the water permeability of membranes increased ~3.2 times. In a follow-up study, the effects of minimizing structural parameter of hollow fiber membranes on AqpZ incorporation were studied with a focus on FO applications [27].

In the present work, we report on the fabrication of hollow fiber membranes with integrated AqpZ proteoliposome on outer surface of hollow fiber membranes which constitutes the most novel part of the study and evaluation of nanofiltration performance of these membranes. Second novelty of the study is evaluating the interactions of AqpZ proteoliposomes using three different types of UF HF supports (polymeric, nanocomposite and reinforced) and determining the effectiveness of the AqpZ proteoliposome immobilization on different UF supports. Separation performance of the obtained Aquaporin-enabled NF membranes in bench-scale tests using feed water with different contents of salts and dissolved organics were performed for this purpose.

2. Materials and Methods

2.1. Materials

Polysulfone (PS, Ultrason S6010) (BASF) and polyvinylpyrrolidone (PVP) (ISP) were used as the UF support polymer and the porogen, respectively. PVP 360 (360 kDa) was used to prepare regular and nanocomposite UF support layers while PVP 40 (40 kDa) was used to make the reinforced UF support. N-Methyl-2-pyrrolidone was used as a solvent (Sigma-Aldrich). The nanocomposite UF support layers contained multiwalled carbon nanotubes (MWCNT) with an outer diameter of < 8 nm (NanoAmor).

Anhydrous piperazine (PIP, ≥99.0%) as amine monomer, trimesoyl chloride (or 1,3,5-benzenetricarbonyl trichloride, TMC, 98%) as acyl monomer, anhydrous cyclohexane (≥99.0%) (Sigma-Aldrich) were used for interfacial polymerization reaction. $MgSO_4$, NaCl, humic acid (HA) and tannic acid (TA) were used to prepare feed solutions for membrane testing. 1,2-dioleoyl-sn-glycero-3-phosphocholine (DOPC) was purchased from Avanti Polar Lipids (Alabaster, AL) to be used for proteoliposome fabrication. Tris-HCl, NaCl, 1- n-octyl-β-d-glucopyranoside (OG) and glycerol were used in purification of AqpZ (Sigma Aldrich). Commercial aquaporin Z (catalog # MBS1117749) (com.AqpZ) was purchased from Mybiosource (San Diego, USA). AqpZ was used as a positive control and was purified from *E. coli* O6 strain. Commercial AqpZ had a concentration of 1.145 mg/mL. Dodecyl maltoside (DDM) (Avanti polar lipids) was used as surfactant for the incorporation of AqpZ into the liposome structure.

2.2. AqpZ cloning, expression and purification

The gene coding for AqpZ of *E. coli* DH5α was amplified by PCR using forward (GGCATATGATGTTCAGAAAATTAGCAGCT) and reverse (TTGAATTCTTAATCACGCTTTTCCAGCA) primers which includes NdeI and EcoRI (Promega, USA) restriction sites, respectively. Following the amplification, the insert and the vector (pET-

28a(+), Novagen, USA) were digested with NdeI and EcoRI. The insert was ligated to dephosphorylated vector and transformed into *E. coli* C43 (DE3) (Lucigen, USA). For expression studies, 500 mL of Luria-Bertani (LB) medium supplemented with 20 µg/mL kanamycin was inoculated with 15 mL of overnight culture of single colony. When OD_{600nm} reached the 0.6 to 0.8 range, protein expression was induced by 1mM IPTG for 4 hours. Purification was done according to [28]. Detailed procedure is given in Supplementary Information (SI). Verification of AqpZ expression and purification by sodium dodecyl sulfate gel electrophoresis (SDS-PAGE) is presented in Figure S1.

2.3. Fabrication of UF HF support layers

Dope solution was made up of 16 wt. % PS, 10 wt. % PVP and 74 wt. % NMP. Prior to use, PS was dried at 100°C for 2 h. PS and PVP were added to NMP and mechanically mixed until no aggregates were observed. To prepare the nanocomposite UF dope solution, 0.01 wt. % MWCNT was added to NMP and sonicated for 30 min at 50 kW. A mixture of 70 wt. % NMP and 30 wt. % water was chosen as the bore solution. First PS and then PVP were added to the solution and mechanically mixed. Residual bubbles in the dope solution were removed by applying vacuum.

Spinning parameters (Table 1) for pristine and nanocomposite UF support layers were optimized as described previously [29, 30]. Spinning parameters for the reinforced UF support layer were then optimized. Briefly, for UF support layer fabrication wet phase inversion method was used. Dope and bore solutions were pumped to the spinneret by nitrogen gas at 2 atm. Combined solutions entered the coagulation bath, the formed fiber was passed to the second coagulation bath, and then collected on the take-up roll. For reinforced UF support layer fabrication, procedure for spinning was the same except no bore fluid was used. Instead a textile fiber was used and the membrane was formed on these fibers. All UF support layers were treated with NaOCl to remove residual PVP from the membrane matrix.

Table 1. Spinning parameters during fabrication of UF support layers.

Spinning parameters	Pristine UF	Nanocomposite UF	Reinforced UF
Coagulation bath temperature, °C	45	45	45
Air gap length, cm	0	0	0
Take-up rate, m/s	0.105	0.105	0.033
Dope extrusion rate, mL/min	6	6	1
Bore liquid flow rate, mL/min	3	3	-

2.4. Fabrication of hollow fiber nanofiltration membranes

Three different UF support layers were used to fabricate HF NF membranes with integrated AqpZ. Pristine (i.e. pure polymer), MWCNT-based nanocomposite and reinforced HF UF support layers had specific permeate fluxes of 309 LMH/bar, 231 LMH/bar, 450 LMH/bar, respectively. BSA rejections by these UF membranes were 82 %, 58 %, 54 %, respectively, confirming that the membranes were in the UF range.

PIP in the aqueous phase (2 % (w:v)) and TMC in organic phase (0.2 % (v:v)) were chosen for the interfacial polymerization reaction [31]. AqpZ reconstituted proteoliposomes (procedure is described in SI) were added to the aqueous phase. HF UF support membranes were soaked in aqueous solution for 2 min to ensure PIP monomer diffusion into the porous support. Residual PIP monomer was removed by applying nitrogen gas at 1 atm for 1 min, and subsequently soaked in a cyclohexane solution for 1 min. The membranes were then immersed into TMC solution for 1 min to complete the polymerization reaction. Finally, membranes were post-treated at 50°C for 5 min. For brevity, membranes are denoted as described in Table 2.

Figure 1 schematically outlines the preparation procedures for HF NF membranes with integrated Aquaporin Z (either cloned or commercial). Polyamide layer was formed on outer surface of all HF membranes.

Table 2. Nomenclature used to denote fabricated HF NF membranes.
[#] No NF layer.
[##] Only monomers added during interfacial polymerization.

Type of UF support	Type of dense NF layer			
	UF support only [#]	**Conventional TFC [##]**	**Cloned AqpZ incorporated**	**Commercial AqpZ incorporated**
Pristine	p-UF	p-TFC	p-AqpZ	p-com. AqpZ
Nanocomposite	CNT-UF	CNT-TFC	CNT-AqpZ	CNT-com.AqpZ
Reinforced	r-UF	r-TFC	r-AqpZ	r-com.AqpZ

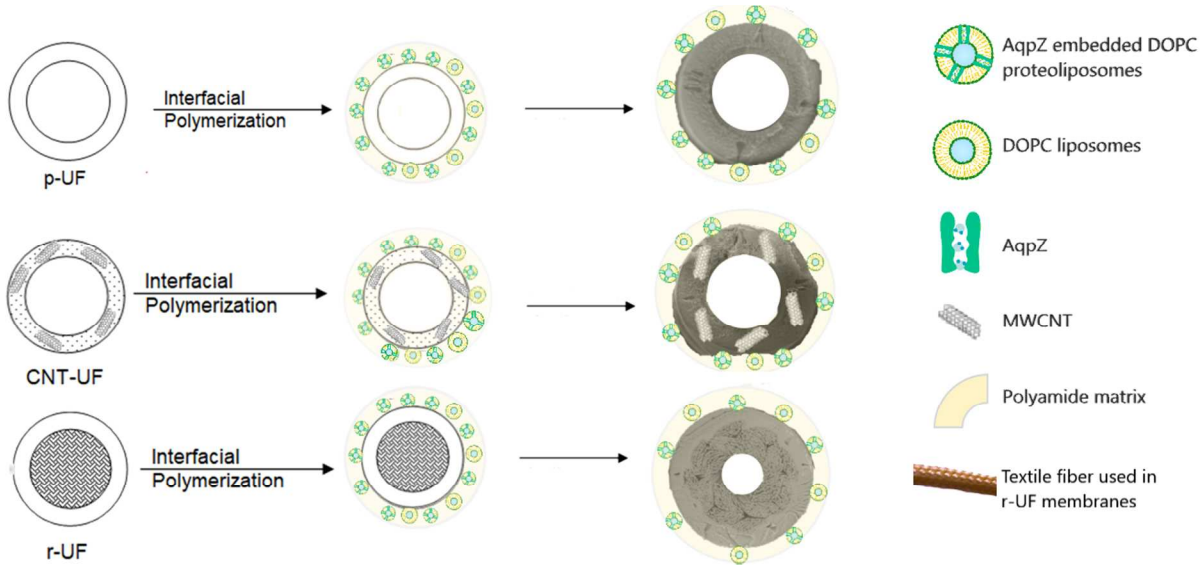

Figure 1. Schematic of preparation of HF NF membranes with integrated Aquaporin Z (either cloned or commercial) in the NF dense layer.

2.5. Characterization of liposomes and proteoliposomes

Nanosizer NanoZS (Malvern, UK) was used to measure the size of liposomes and proteoliposomes. Stopped-flow apparatus (SX20, Applied Photophysics, UK) was used to determine water permeability of liposomes and proteoliposomes. Liposomes and proteoliposomes were rapidly mixed with hyperosmolar sucrose solution having Δ_{osm} of 926 mOsmol/L (determined by Advanced Instruments 3250 Osmometer (UK)) to measure the rate of vesicle shrinkage by light scattering [13, 19, 32]. (Osmolarity measures the number of osmoles of the solute particles per unit volume of solution allowing the measurement of osmotic pressure of a solution and determining how diffusion will occur between liposomes and sucrose solution). The

osmotic water permeability of vesicles, P_f was determined according to the following equation [27]:

$$P_f = \frac{k_0}{\frac{S_0}{V_0} V_w \Delta_{osm}} \quad (1)$$

where S_0 and V_0 stand for the initial surface area and the initial volume of vesicles, respectively; V_w is the partial molar volume of water (18 cm^3/mol) and Δ_{osm}(osmol/L) is the osmolarity difference that ensures the shrinkage of vesicles.

2.6. Characterization of fabricated HF NF membranes

Membrane morphology was evaluated using FEI Quanta FEG 200 scanning electron microscope (SEM). The samples were coated with Pd and Au prior to imaging (Quorum SC7620 ion sputtering machine). FTIR spectroscopy (Spectrum 100, PerkinElmer, USA) was used to assess changes occurred the chemical composition of the membranes after interfacial polymerization.

2.7. Determination of HF NF membrane performance

2.7.1. Observed rejection

Cross-flow filtration tests were used to assess nanofiltration performance of the membranes. The cross-flow rate was maintained constant at 250 mL/min and three different pressures were used (3, 4, and 5 bars). The crossflow velocity was within 2.11 cm/s - 2.14 cm/s range depending on the number of hollow fibers in the module. Solutions of $MgSO_4$ (1000 ppm (8.3 mM)) and NaCl (1000 ppm (17.1 mM)) in DI water were used as the feed. The membranes were first compacted by filtering DI water at 3 bars for 1 h to ensure stable permeate flux. Then, NF water flux, J_w, and observed salt rejection, R_{obs}, were calculated. Hach conductivity probe was used to measure conductivity.

2.7.2. Intrinsic rejection

Mass transfer coefficient, k, for $MgSO_4$ and NaCl salt solutions in the hollow fiber membrane module was estimated using correlation derived by Yang and Cussler for shell-side mass transfer [33] to characterize the selectivity of the membranes (eq. 2);

$$Sh = \frac{kd_h}{D} = 1.25\left(Re\frac{d_h}{L}\right)^{0.93} Sc^{0.33} \quad (2)$$

where Sh is the Sherwood number, L is the length of the hollow fiber, D is the diffusion coefficient of the solute in water ($8.5\cdot10^{-10}$ m^2/s for $MgSO_4$ and $1.6\cdot10^{-9}$ m^2/s for NaCl [34]), Re is the Reynolds number, Sc is the Schmidt number, and d_h is the hydraulic diameter of the hollow fiber module. Schmidt number is equal to $\mu/(\rho D)$ whereas Reynolds number is equal to $d_h v\rho/\mu$ where μ and ρ are the viscosity and density of water, respectively. The correlation is valid for the fiber packing density in the range from 2.5 % to 40 %.

For the estimation of the concentration of salt at the membrane surface, C_m, thin film model was used [24] (eq. 3):

$$\frac{C_m - C_p}{C_f - C_p} = exp\left(\frac{J}{k}\right) \quad (3)$$

where C_p, C_f, and C_m are the concentrations of the salt in the permeate, in the bulk feed, and in the portion of the feed directly adjacent to the membrane, respectively. The right hand side of eq. (3) gives the concentration polarization factor. The intrinsic rejection, R_{int}, as a function of the permeate flux, J, is given by eq. 4:

$$R_{int} = 1 - \frac{C_p}{C_m} \quad (4)$$

In this study, three different transmembrane pressure differentials ΔP, were used and values of R_{int} were determined as a function of J using eq. (4).

2.7.3. Determination of TOC rejection

Humic (HA) and tannic (TA) acids were selected to represent hydrophobic and hydrophilic components of natural organic matter [35], respectively. Concentrations of HA and TA in the feed were adjusted to 5 mg/L. Measurements of the total organic carbon (TOC) (Shimadzu) and UV-vis absorption (Hach Lange spectrophotometer) were used to quantify the removal of organic matter. Diffusion coefficients of HA and TA needed for the estimation of intrinsic rejection of organics were measured using Nanosizer (Malvern Instruments).

3. Results and Discussion

3.1. Proteoliposome characterization

Table 3 summarized results of particle size measurements with liposome and proteoliposome suspensions. Reconstitution of either cloned or commercial AqpZ into liposomes did not affect the vesicle size, possibly due to low protein incorporation. PDI of vesicles was below 0.15 for all samples indicating that the suspensions were close-to-monodisperse. Raw size distribution data is given in Figure S2.

Table 3. Mean diameter and polydispersity of liposomes and proteoliposomes.

Liposome solution	Mean diameter of vesicles (nm)	Polydispersity index (PDI)
DOPC	167 ± 11	0.090 ± 0.031
DOPC: cloned AqpZ	176 ± 11	0.113 ± 0.049
DOPC: commercial AqpZ	166 ± 12	0.074 ± 0.041

Figure 2 shows normalized intensity of scattered light measured in stopped-flow tests and water permeability of DOPC liposome and proteoliposomes. By fitting data to a single exponential function [36] kinetic rate constants were calculated to be 15.6 ± 1.9 s^{-1}, 44.1 ± 8.5 s^{-1} and 52.8 ± 10.8 s^{-1} for DOPC, DOPC: AqpZ and DOPC:com.AqpZ, respectively. The low kinetic constant of DOPC corresponded to low water permeability, which was consistent with the data reported by Sun et al. [13]. In contrast, addition of AqpZ increased the kinetic constant (~ 3 times) and water

permeability (~ 3.3 times) of proteoliposomes for cloned AqpZ and commercial AqpZ, approximately. Proteoliposomes prepared in this study had almost 17 times lower water permeability compared to values reported earlier [24, 27]. Lower water permeability of proteoliposomes may be related to the low protein incorporation, the use of low AqpZ content for reconstitution into DOPC. Since M_w of AqpZ approximately 24 kDa, if molar ratio is used for proteoliposome preparation, AqpZ amount needed will be much higher. This can improve reconstitution of AqpZ within liposomes [37]. Other important factors that may explain the low water permeability include low yield of AqpZ reconstitution typical for detergent-mediated methods, nature of the detergent, the choice of the procedure for proteoliposome reconstitution (e.g. not using freeze-thaw method), rate of detergent removal, nature of the protein, protein conformations and lipid composition [38].

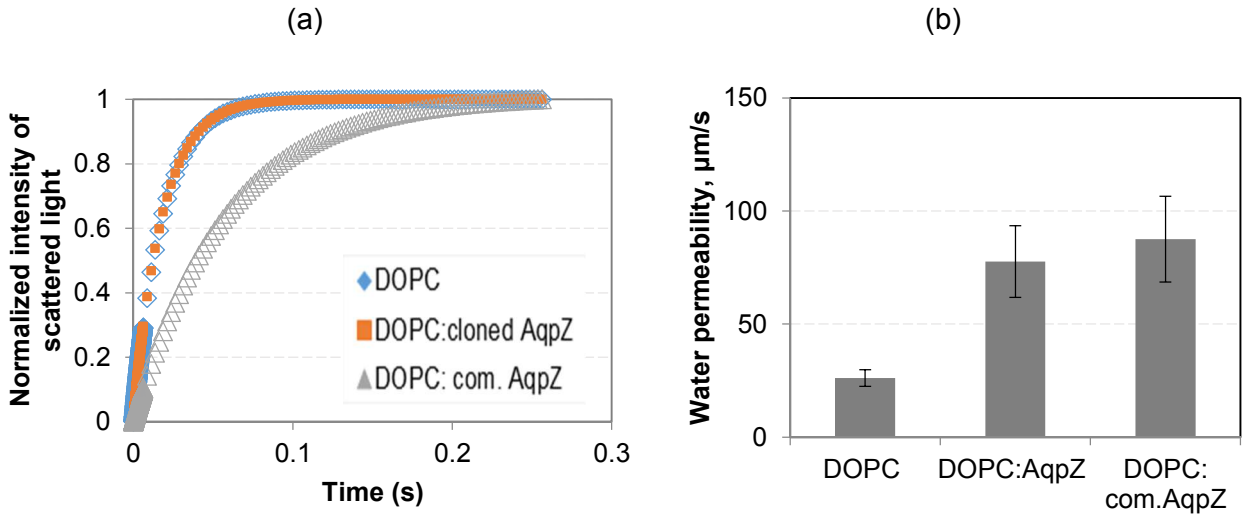

Figure 2. Normalized intensity of scattered light in stopped-flow tests (a) and water permeability of DOPC-based liposomes and proteoliposomes (b).

3.2. Surface characteristics of membranes

As SEM images indicate (Figures 3 and S3) the morphology of the polyamide layer depended on the type of UF support. For reinforced NF membranes, the polyamide layer had worm-like surface morphology. It is known that PIP reaction with TMC leads to a polyamide layer with

valley-and-ridge morphology [39]. Because PIP interaction with TMC is fast [40], the effect of the support type can be to accelerate or retard PIP diffusion towards TMC solution. Nodules that are small but high in number can be seen in p-AqpZ and CNT-AqpZ layers whereas fewer and larger nodules are found in CNT-TFC and CNT-com.AqpZ layers.

The morphology of membranes with AqpZ differed from that of the AqpZ-free polyamide layer. For all membranes with AqpZ (either cloned or commercial), membrane surfaces were successfully covered with AqpZ embedded proteoliposomes. Some globular proteoliposomes were also detected. Further, the size of these unruptured vesicles in the polyamide layer was similar (177 nm, 188 nm for r-AqpZ and r-com.AqpZ; 146 nm, 175 nm for CNT-AqpZ and CNT-com.AqpZ; 168 nm, 198 nm for TFC-AqpZ and TFC-com.AqpZ) to the vesicle size measured by dynamic light scattering (167 nm, 176 nm and 166 nm for DOPC, DOPC : AqpZ and DOPC : com.AqpZ, respectively).

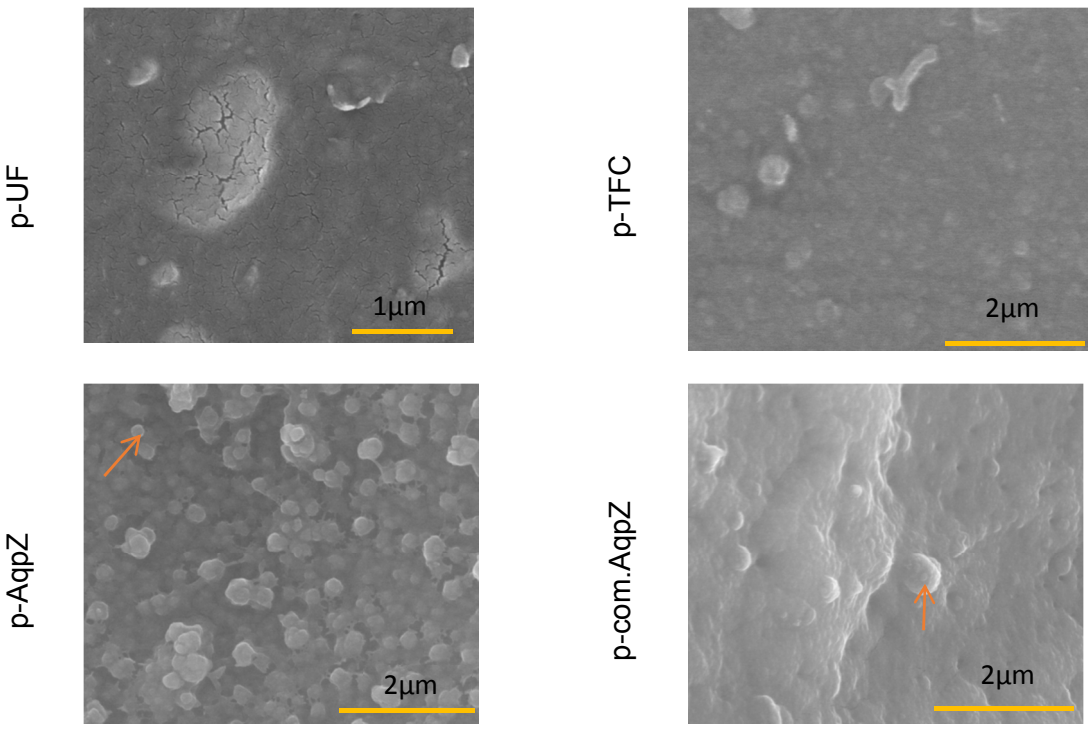

Figure 3. SEM images of fabricated HF NF membranes: Planar view of the separation layer.

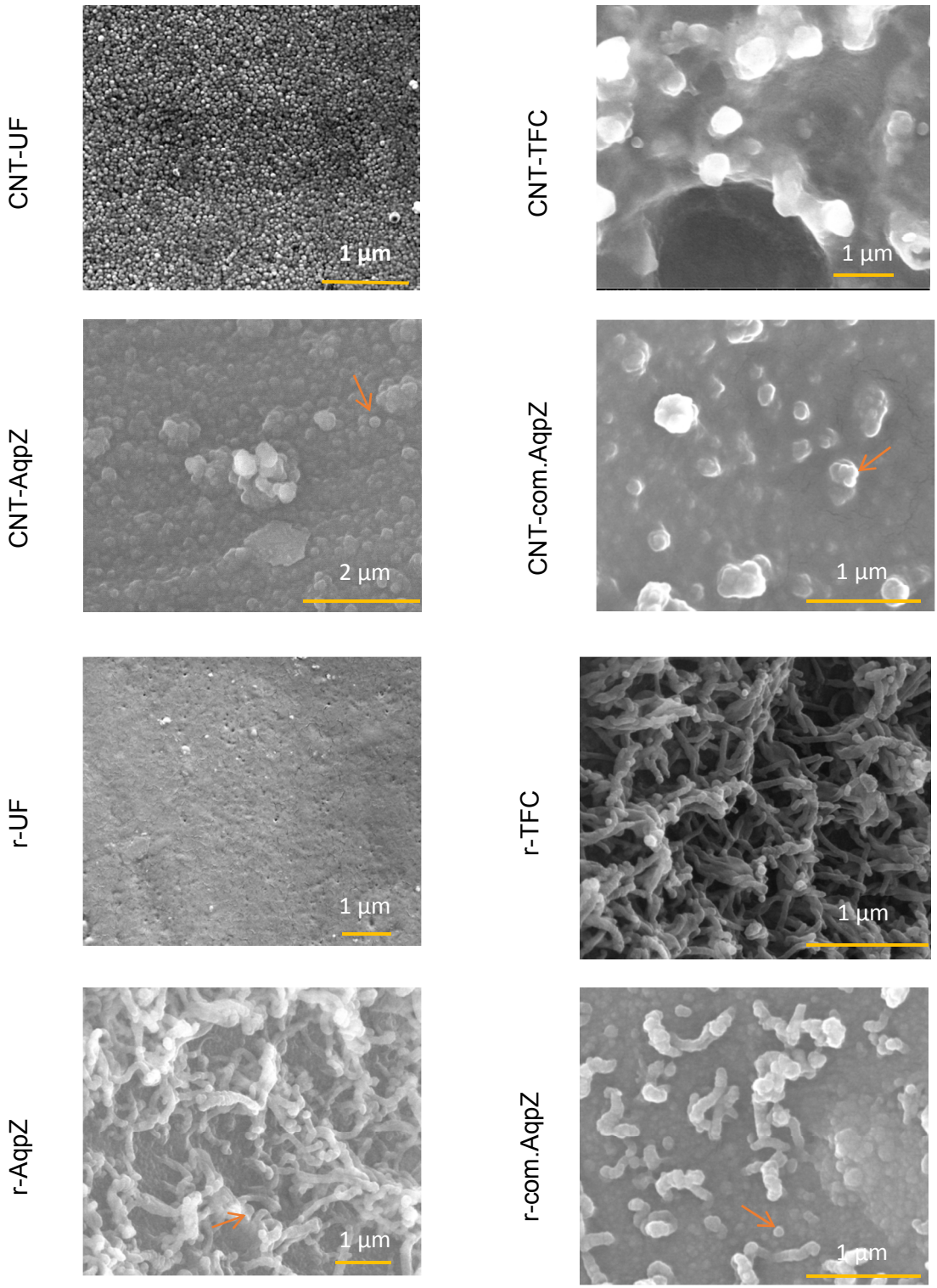

Figure 3 (continued): SEM images of fabricated HF NF membranes: Planar view of the separation layer.

Contact angles of water on p-UF, CNT-UF and r-UF supports were 75.0° ± 6.0°, 81.0° ± 5.0° and 70.0° ± 5.0°, respectively (Figure 4). Hydrophilicity has an effect on the binding between the substrate and the active layer. Yang et al. [41] showed that higher surface hydrophilicity can increase wettability with amine solution as well as binding between substrate and active layer due to better compatibility. In this study, the reinforced support layer had better compatibility between monomers so that binding between active layer and support layer was probably the strongest among all membranes (except r-com.aqpZ membrane). Including AqpZ improved surface hydrophilicity of the membranes (except r-com.AqpZ), which was consistent with the trend observed by Wang et al. [42].

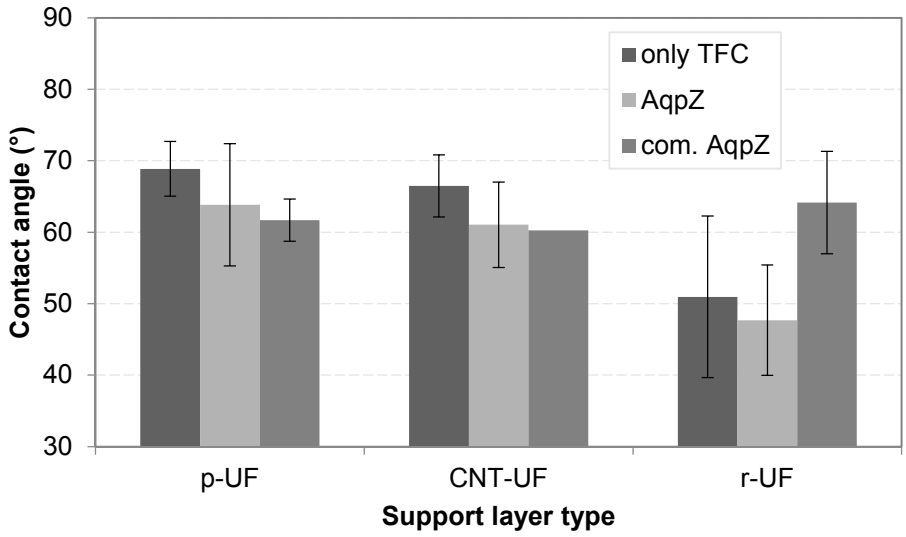

Figure 4. Water contact angle values for fabricated HF NF membranes prepared on different support layers.

Surface roughness of membranes was determined using optical profilometer (Figure 5). A decrease in surface roughness was expected due to the smaller number of in worm-like and ridge-valley structures. Wang et al. [17] found that incorporation of AqpZ decreased surface roughness by filling the gaps in substrate. However, in the present study incorporation of either cloned or commercial AqpZ into polyamide layer was found to increase surface roughness

(except for p-com.Aqpz and CNT-AqpZ). One possible reason for the increased surface roughness could be the existence of unruptured proteoliposomes on the membrane surface.

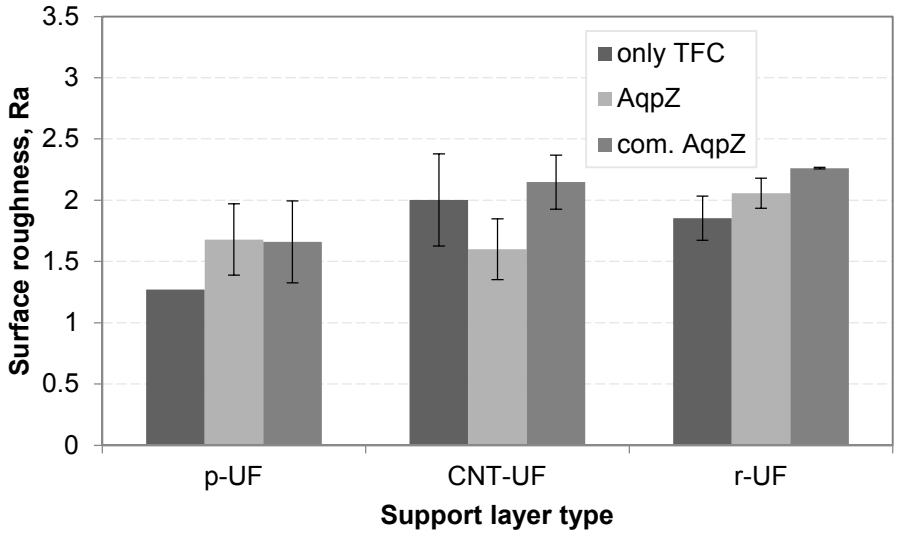

Figure 5. Surface roughness of fabricated HF NF membranes.

FTIR spectra of membranes with integrated AqpZ (Figure S4) show fingerprint peaks of DOPC P=O (asymmetric stretching vibration), P-O-, C-C-N^+ and C-H-C, which can be found in 1232 cm^{-1}, 949 cm^{-1}, 716 cm^{-1} and 2900 cm^{-1}, respectively (Figure S5).

3.3. Determination of Membrane Performance

3.3.1. Water Permeability

Figure 6 presents specific permeate flux values for all nine membranes tested in this study. Integration of AqpZ lead to a statistically significant ($p < 0.01$) increase in the specific flux for p-AqpZ membrane by the factor of ~ 2.5. Integrating com.AqpZ into the same membrane (p-AqpZ) led to a somewhat smaller increase (~ 2.2 times), which was statistically significant with only 90% confidence ($p < 0.1$). The surface density of water channels can be low in membranes where specific permeate flux of membrane was not improved. Low surface density of water

channels may decrease the probability of water molecules able to come into contact with protein water channels [32].

When modifying the polyamide matrix on CNT-UF supports the specific flux could be enhanced by com.AqpZ (~1.6 times; ($p < 0.05$)) but not by AqpZ ($p > 0.1$)). Since water permeability of cloned AqpZ was higher than com.AqpZ, higher specific fluxes were expected for membranes with cloned AqpZ, which was indeed the case except for CNT-AqpZ membranes. This may be related to the incomplete removal of PVP from membrane matrix by NaOCl treatment. It is known that additives such as PVP and PEG can interact with amine monomers during interfacial polymerization and reduce membrane performance. Thus, even though CNT-AqpZ membrane had proteoliposomes in its structure, interaction between PVP and PIP could have suppressed AqpZ function [43].

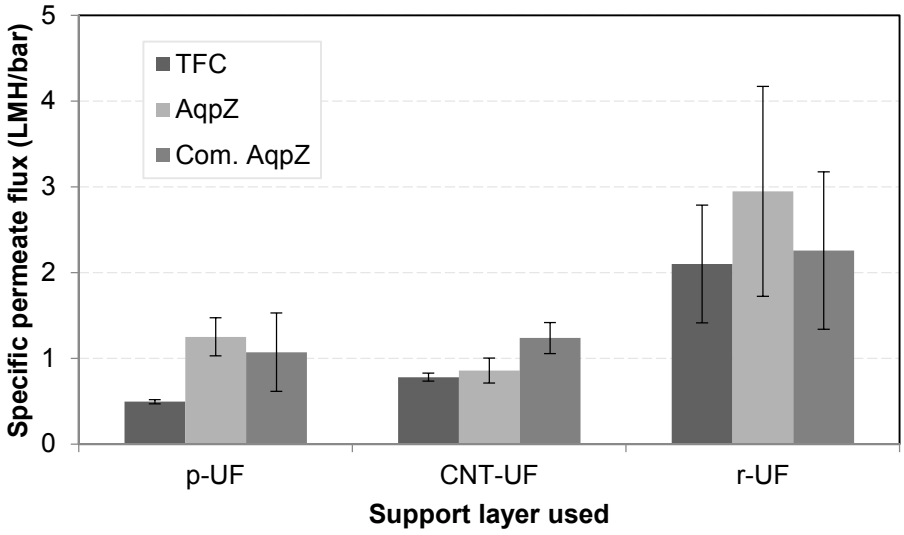

Figure 6: Specific permeate flux measured for the nine types of membranes evaluated in this study. In all tests the transmembrane pressure was 1 bar.

The highest average flux values were obtained with reinforced membranes. However, changes in the permeate flux of the TFC layer on r-UF support by the integration of AqpZ and com.AqpZ

were not statistically significant ($p = 0.355$ and $p = 0.824$, respectively). This trend is attributed to the low channel density on the membrane surface [44].

It should be also noted that, specific permeate flux differences for different supports can be related to the large irregularities in the membrane structure and likely large differences from one membrane to another. This phenomenon may also affect the stability of proteoliposomes and total number of proteoliposomes functionally encapsulated in polyamide layer.

3.3.2. Determination of $MgSO_4$ and NaCl rejection of NF HF membranes with integrated AqpZ

To determine membrane selectivity with respect to $MgSO_4$ and NaCl, observed and intrinsic rejections were determined. Observed rejection data for $MgSO_4$ and NaCl was given in Figure S6 and Figure S7, respectively. On the other hand, for p-UF and CNT-UF used membranes, packing densities of the modules were below the 2.5% - 40% range where Yang and Cussler model for shell-side mass transfer is applicable. No other model could be found for fiber packing densities below 2.5%. Therefore, intrinsic rejections were calculated only for reinforced NF membranes. In Figure 7 comparison data for observed and intrinsic rejections of $MgSO_4$ and NaCl salts were presented. The data showed that all reinforced membranes were affected by concentration polarization.

When the effects of AqpZ integration and support layer were investigated, it can be seen that for all membranes water permeate flux increased as AqpZ was incorporated into polyamide matrix (except r-com. AqpZ NaCl flux) at 5 bars (Figure S6 and Figure S7). In general, r-UF support used NF membranes had higher water permeate fluxes which was related to stability of r-UF to pressure without getting flattened. Although no result was presented here, p-UF and CNT-UF membranes cannot withstand pressures slightly higher than 5 bars whereas reinforced membranes can withstand 6 bars (System pressure can be set maximum to 6 bars). Water

permeate fluxes increased linearly with the applied pressure and salt rejections were enhanced at higher pressures as expected when r-UF membranes were used. Improved salt rejections can be related to the fact that greater fluxes at higher pressures helps to reduce permeate solute concentration by dilution effect [19].

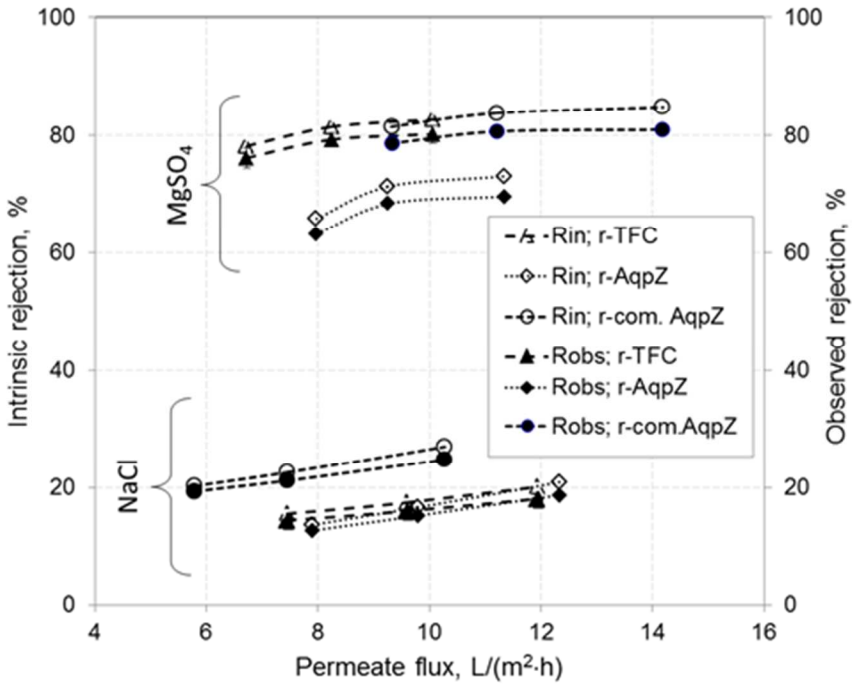

Figure 7: Intrinsic rejection vs. observed rejection comparison of fabricated membranes for $MgSO_4$ and NaCl salts. Lines are added to guide the eye.

3.3.3. Determination of organic matter removal of NF HF membranes with integrated AqpZ

Humic acid and tannic acid were chosen as organic foulants to represent different natural organic matter (NOM) structures. Soil based humic acid is more hydrophobic and tends to have a larger average molecular weight compared to river based humic acid [45]. On the other hand, tannic acid consists of significant amounts of saccharides and aromatic acid compounds which reflect some of organic materials in surface waters [46].

Figure 8 and Figure S8 present permeate flux and rejection after the membranes are fouled by HA and TA. Initial permeate flux values were measured to be 1.69 L/m^2.h, 4.24 L/m^2.h, 2.79 L/m^2.h, 2.31 L/m^2.h, 1.53 L/m^2.h, 1.28 L/m^2.h, 7.95 L/m^2.h, 5.81 L/m^2.h and 3.99 L/m^2.h for TFC, TFC-AqpZ, TFC-com.AqpZ, CNT-TFC, CNT-AqpZ, CNT-com.AqpZ, r-TFC, r-AqpZ and r-com.AqpZ membranes, respectively. TOC removal efficiencies were lower than UV_{254} removal efficiencies for all cases. The differences between removal efficiencies of TOC and UV_{254} may be resulted from the fact that each method measures different type of compounds. TOC oxidation efficiency is higher for smaller and more aliphatic compounds whereas UV_{254} is better absorbed by large aromatic compounds. Therefore smaller aliphatic compounds have ability to pass through the membrane more easily than larger aliphatic compounds [47]. Nine membranes were fabricated with either cloned or commercial AqpZ. For two membranes TOC values were found lower than TFC membranes (efficiency loss between 6.4% to 59 % for HA) whereas for four membranes UV_{254} values were found lower than TFC membranes (efficiency loss between 1.4 % to 21.6 % for HA). Highest efficiency losses were obtained for CNT-UF membranes. On the other hand, fouling properties of membranes were investigated, no water permeate flux decrease was observed for HA filtration (except CNT-com.AqpZ). Flux decrease after organic matter filtration by CNT-com.AqpZ membrane can be explained by a higher concentration polarization. Highest water permeate flux increase was reached CNT-AqpZ membranes as 120%.

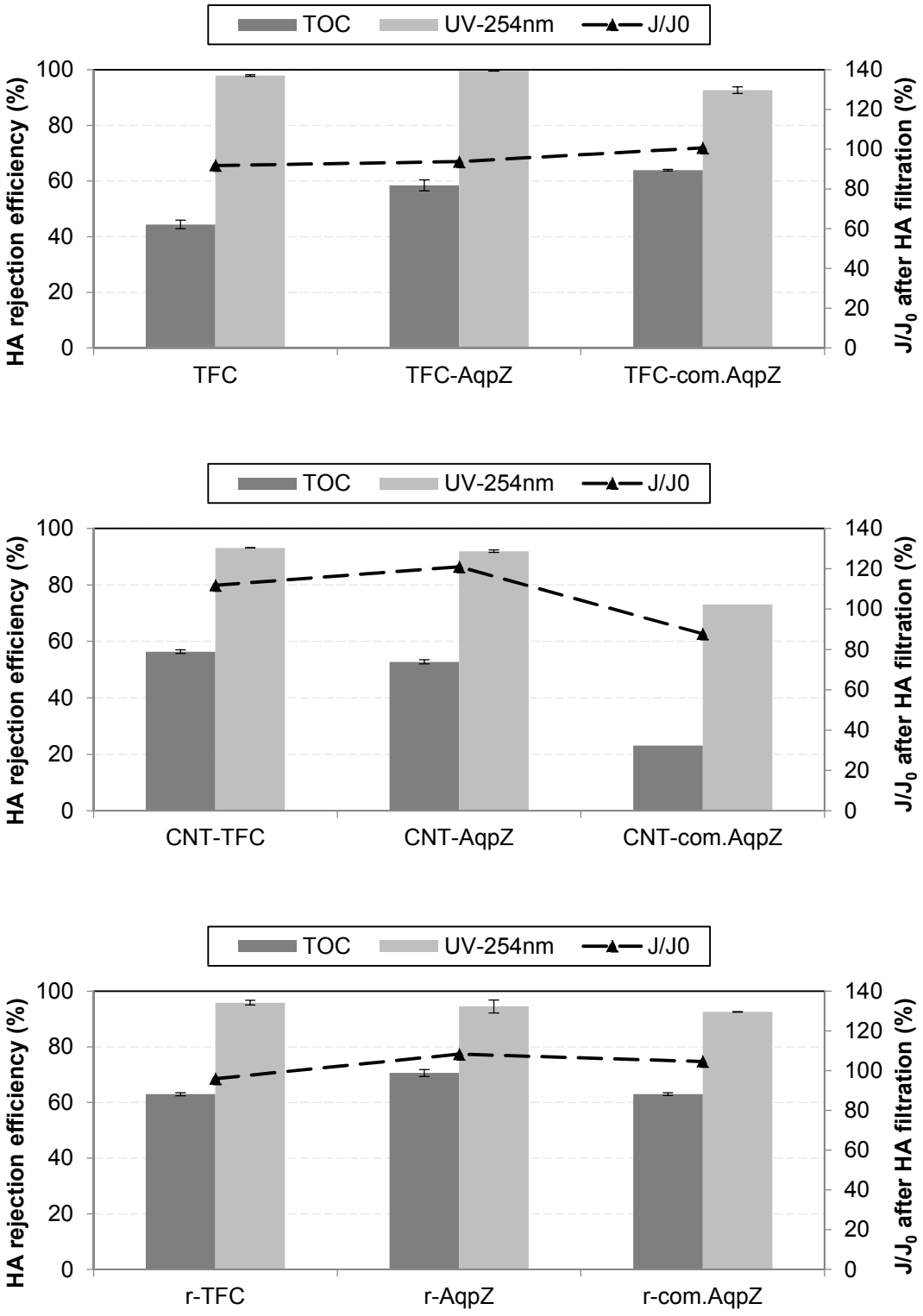

Figure 8: Normalized permeate flux and HA rejection by fabricated nanofiltration membranes based on a) p-UF, b) CNT-UF, c) r-UF support layers.

3.3.4. Benchmarking of the fabricated membranes

Membrane's performance was benchmarked using the Figure of Merit, (eq. (5))

$$FOM = \frac{J}{\Delta P} * R_n * \frac{J}{J_{0_n}} \quad (5)$$

where $J/\Delta P$ is the specific permeate flux of pure water, R_n is the rejection of TA or HA, and J/J_{0n} is the flux recovery ratio defined as permeate flux after filtration of NOM-containing feed divided by the initial permeate flux. Figure 9 presents FOM data based on experiments with HA. (Corresponding data for TA is given in Figure S9.) All membranes had FOM higher than that of p-TFC membrane. Thus, the FOM of p-TFC was taken to be 1 and used as the comparative basis for all other membranes. Cloned AqpZ increased membrane performance more than commercial AqpZ did. Among the nine membranes tested, r-AqpZ membrane had the highest FOM value.

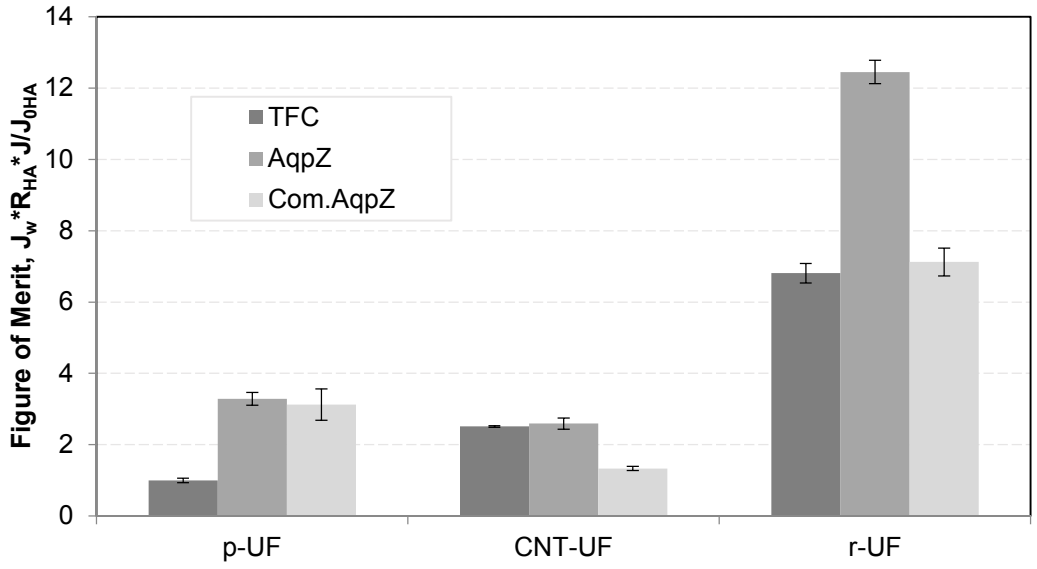

Figure 9: Figure of Merit (see eq. 5) for the nine membrane types evaluated in this study. The values are based on experiments with HA and normalized by the Figure of Merit of the p-TFC membrane.

Table 4 summarizes flux and rejection performance of AqpZ integrated membranes as reported in the published literature. Although water permeability of AqpZ reconstituted proteoliposomes in the present work is the lowest, the pure water permeability and salt rejections by membranes with integrated AqpZ are competitive with those reported earlier. We conclude that the performance of AqpZ integrated hollow fiber membranes can be improved by optimizing UF support properties, by adjusting interfacial polymerization conditions, by increasing the amount of AqpZ content for the reconstitution into liposomes.

4. Conclusions

This study examined the effects of the hollow fiber ultrafiltration support on the performance of AqpZ integrated hollow fiber nanofiltration membranes. Interfacial polymerization was used to integrate AqpZ embedded proteoliposomes into the polyamide layer. Water permeabilities of AqpZ embedded proteoliposomes were determined by stopped flow experiments. SEM and FTIR results showed that successful incorporation of AqpZ into polyamide matrix. Surface characteristics, membrane permeability and selectivity were found to be changed with the type of UF support layer used. While integration of AqpZ into polyamide matrices increased their permeability to water, the rejection performance of the membranes decreased at least 10 %. Compared to AqpZ-free thin film composite membranes, performance of the AqpZ integrated NF membrane on a reinforced UF support was higher 9 to 12 fold as measured in terms of the Figure of Merit, which is an aggregate metric of membrane performance that includes water permeability, selectivity and resistance to fouling. In sum, the study illustrates the potential AqpZ based hollow fiber membranes in nanofiltration. Embedding AqpZ to achieve higher separation performance adds on to such advantages of hollow fiber membranes as high packing density, small footprint and energy demand. The use of reinforced UF supports enhances the mechanical stability of hollow fiber membranes to improve their reliability in higher pressures applications.

Table 4: Comparison of hollow fiber membranes with integrated AqpZ against that of similar membranes from the published literature.

Module type	AqpZ incorporation method	Water permeability of proteoliposome (μm/s)	Pure water permeability (LMH/bar)	Salt rejection (%)	Membrane area	Testing conditions	Ref.
FS*	Silanization	2049	27.86±4.16	21.76±7.79	3 mm^2	5 bar, 200 ppm NaCl, PMOXA-b-PDMS-PMOXA polymer vesicle, 100:1 lipid to protein ratio (LPR) n.a.	32
FS	Polymer crosslinking	266	~27	~91	28.3 cm^2	1 bar, 100 ppm MgCl2, DOPC liposomes, 400:1 LPR n.a.	12
FS	Vesicle spreading on alumina substrate	~3000	16.1±3.3	45.1±4.2	0.2 cm^2	5 bar, 200ppm NaCl, disulfide-functionalized PMOXA-PDMS-PMOXA polymer vesicles, 100:1 LPR molar ratio	11
FS	Amidation	~550	22.9±3.3	51.0±7.0	n.a.	5 bar, 200 ppm NaCl, PMOXA-PDMS-PMOXA block copolymer polymer vesicles, 200:1 LPR molar ratio	18
FS	Self-assembly	~500±100	4.8±0.4	90.0±1.0	78.5 mm^2	4 bar, 200 ppm $MgCl_2$, POPC/POPG/Chol liposomes, 100:1 LPR n.a.	15
FS	Polyelectrolyte self-assembly	2537	~14.0±0.5	~75.0±2.0	19.6 cm^2	4 bar, 500 ppm NaCl, DOPC/DOTAP liposomes, 200:1 LPR w:w ratio	17
FS	Interfacial polymerization	600	4	97	42 cm^2	5 bar, 355ppm NaCl, DOPC liposome, 200:1 LPR molar ratio	19
FS	Vesicle spreading	n.a.	~4.8±0.2	~20.0±4.0	n.a.	1 bar, 1 mM NaCl, DOPC liposome, 200:1 LPR molar ratio	36
FS	PDA deposition and crosslinking	242	~3.0±0.5	~68.0±3.0	0.8 cm^2	5 bar, 200 ppm NaCl, DOPC, DSPE-PEG-NH2, EGDMA and UV initiator Irgacure 184 liposomes, 100:1 LPR w:w ratio	13

FS	Interfacial polymerization	1000	4.1±0.4	97.2±0.6	42 cm^2	10 bar, 10 mM NaCl, E.Coli lipid n.a.	[48]
FS	Amide linked PDA coating	1335	6.3	90	36 cm^2	4 bar, 2000 ppm NaCl, DOPE/DOTAP liposomes, 100:1 LPR molar ratio	[49]
HF**	Interfacial polymerization	1000	7.6±0.5	90.0±2.0	38 cm^2	1 bar, 500 ppm NaCl, E.Coli lipid, 100:1 LPR n.a.	[27]
HF	Interfacial polymerization	~1600±150	~7.8±0.2	~90.0±2.0	34.2 cm^2	5 bar, 500 ppm NaCl, DOPC liposome, LPR n.a.	[24]
HF	Interfacial polymerization	77.6	3.2±1.1	69.6±16.5 18.8±2.7	25±10 cm^2	5 bar, 1000ppm $MgSO_4$ and NaCl, DOPC liposome, 100:1 LPR w:w ratio	This work
HF	Interfacial polymerization	77.6	1.2±0.2	60.9±5.4 16.3±5.6	25±10 cm^2	5 bar, 1000ppm $MgSO_4$ and NaCl, DOPC liposome, 100:1 LPR w:w ratio	This work
HF	Interfacial polymerization	77.6	0.8±0.13	72.5±5.4 24.6±0.8	25±10 cm^2	5 bar, 1000ppm $MgSO_4$ and NaCl, DOPC liposome, 100:1 LPR w:w ratio	This work

*FS: Flat sheet, **HF: hollow fiber

Conflict of Interests

There are no conflicts of interest to declare.

Acknowledgement

The authors are grateful to TUBITAK (The Scientific and Technological Research Council of Turkey) for the financial support under grant (Project No: 113Y359) and TUBITAK 2211 scholarship program. The work was also supported in part by the U.S. National Science Foundation Partnerships for International Education and Research program under Grant IIA-1243433. Authors thank Abdulhalim Kilic and Fatma Nese Kok for their kind help with liposome preparation as well as Melek Ozkan for her permission to use stopped-flow equipment.

References

1. N. Bolong, A. F. Ismail, M. R. Salimb and T. Matsuura, *Desalination*, 2009, **239**, 229-240.
2. N. Hilal, H. Al-Zhoubi, N. A. Darwish, A. W. Mohamma and M. Abu Arabi, *Desalination*, 2004, **170**, 281-308.
3. M. Kumar, M. Grzelakowski, J. Zilles, M. Clark and W. Meier, *Proc. Natl. Acad. Sci.* , 2007, **104**, 20719-20724.
4. J. S. Hub and B. L. de Groot, *Proc. Natl. Acad. Sci.* , 2008, **105**, 1198-1203.
5. Y. X. Shen, P. O. Saboe, I. T. Sines, M. Erbakan and M. Kumar, *J. Membr. Sci.*, 2014, **454**, 359-381.
6. A. Giwa, S. W. Hasan, A. Yousuf, S. Chakraborty, D. J. Johnson and N. Hilal, *Desalination*, 2017, **420**, 403-424.
7. R. Sengur-Tasdemir, S. Aydin, T. Turken, E. Ates Genceli and I. Koyuncu, *Separation & Purification Reviews*, 2016, **45**, 122-140.
8. C. Tang, Z. Wang, I. Petrinić, A. G. Fane and C. Hélix-Nielsen, *Desalination*, 2015, **368**, 89-105.
9. C. Y. Tang, Y. Zhao, R. Wang, C. Hélix-Nielsen and A. G. Fane, *Desalination*, 2013, **308**, 34-40.
10. J. Habel, M. Hansen, S. Kynde, N. Larsen, S. R. Midtgaard, G. V. Jensen, J. Bomholt, A. Ogbonna, K. Almdal, A. Schulz and C. Hélix-Nielsen, *Membranes*, 2015, **5**, 307-351.
11. P. H. H. Duong, T. S. Chung, K. Jeyaseelan, A. Armugam, Z. Chen, J. Yang and M. Hong, *J. Membr. Sci.*, 2012, **409-410**, 34-43.
12. X. Li, R. Wang, F. Wicaksana, C. Tang, J. Torres and A. G. Fane, *J. Membr. Sci.,*, 2014, **450**, 181-188.
13. G. Sun, T. S. Chung, K. Jeyaseelan and A. Armugam, *Colloids and Surface B*, 2013, **102**, 466-471.
14. G. Sun, T.-S. Chung, N. Chen, X. Lu and Q. Zhao, *RSC Advances*, 2013, **3**, 9178.
15. G. Sun, T.-S. Chung, K. Jeyaseelan and A. Armugam, *RSC Advances*, 2013, **3**, 473.

16. G. Sun, H. Zhou, Y. Li, K. Jeyaseelan, A. Armugam and T. S. Chung, *Coll. Surf. B*, 2012, **89**, 283-288.
17. M. Wang, Z. Wang, X. Wang, S. Wang, W. Ding and C. Gao, *Environ. Sci. Technol.*, 2015, **49**, 3761-3768.
18. W. Xie, F. He, B. Wang, T. S. Chung, K. Jeyaseelan, A. Armugam and Y. W. Tong, *J. Mater. Chem. A*, 2013, **1**, 7592.
19. Y. Zhao, C. Qiu, X. Li, A. Vararattanavech, W. Shen, J. Torres, C. Helix-Nielsen, R. Wang, X. Hu, A. G. Fane and C. Y. Tang, *J. Membr. Sci.*, 2012, **423-424**, 422-428.
20. Y. Kaufman, A. Berman and V. Freger, *Langmuir*, 2010, **26**, 7388-7395.
21. Y. Kaufman, S. Grinberg, C. Linder, E. Heldman, J. Gilron, Y. X. Shen, M. Kumar, R. G. H. Lammertink and V. Freger, *J. Membr. Sci.*, 2014, **457**, 50-61.
22. J. Vogel, M. Perry, J. S. Hansen, P. Y. Bolinger, C. H. Nielsen and O. Geschke, *J. Micromech. Microeng.* , 2009, **19**, 25026.
23. H. Wang, T. S. Chung, Y. W. Tong, W. Meier, Z. Chen, M. Hong, K. Jeyaseelan and A. Armugam, *Soft Matter*, 2011, **7**, 7274.
24. X. Li, S. Chou, R. Wang, L. Shi, W. Fang, G. Chaitra, C. Y. Tang, J. Torres, X. Hu and A. G. Fane, *Journal of Membrane Science*, 2015, **494**, 68-77.
25. S. Engelhardt, A. Sadek and S. Duirk, *Separation and Purification Technology*, 2018, **197**, 170-177.
26. J. Ren and J. R. McCutcheon, *Desalination*, 2018, **442**, 44-50.
27. X. Li, C. H. Loh, R. Wang, W. Widjajanti and J. Torres, *Journal of Membrane Science*, 2017, **525**, 257-268.
28. D. F. Savage, E. P.F., Y. Robles-Colmenares, J. D. O'Connell and S. R.M., *PLOS Biology*, 2003, **1**, 72.
29. E. A. Genceli, R. Sengur-Tasdemir, G. M. Urper, S. Gumrukcu, Z. Guler-Gokce, U. Dagli, T. Turken, A. Z. Sarac and I. Koyuncu, *Polymer Bulletin*, 2017, DOI: https://doi.org/10.1007/s00289-017-2155-3.
30. R. Sengur-Tasdemir, G. M. Urper, T. Turken, E. A. Genceli, V. V. Tarabara and I. Koyuncu, *Separation Science and Technology*, 2016, **51**, 2070-2079.
31. T. Ormanci-Acar, F. Celebi, B. Keskin, O. Mutlu-Salmanlı, M. Agtas, T. Turken, A. Tufani, D. Y. Imer, G. Ozaydin Ince, T. U. Demir, Y. Z. Menceloglu, S. Unal and I. Koyuncu, *Desalination*, 2018, **429**, 20-32.
32. P. S. Zhong, T.-S. Chung, K. Jeyaseelan and A. Armugam, *Journal of Membrane Science*, 2012, **407-408**, 27-33.
33. J. Wu and V. Chen, *J. Membr. Sci.,*, 2000, **172**, 59-74.
34. J. S. Newman, Prentice Hall, 2nd edn., 1991.
35. R. M. Clark and B. K. Boutin, *EPA*, 2001.
36. X. Li, R. Wang, C. Tang, A. Vararattanavech, Y. Zhao, J. Torres and A. G. Fane, *Colloids and Surfaces B: Biointerfaces*, 2012, **94**, 333-340.
37. B. J. Frisken, C. Asman and P. J. Patty, *Langmuir*, 2000, **16**, 928-933.
38. J. L. Rigaud and D. Levy, *Methods in Enzymology*, 2003, **372**.
39. F. A. P. Oreamuno, PhD, Standford University, 2011.
40. B. W. Zhou, H. Z. Zhang, Z. L. Xu and Y. J. Tang, *Desalination*, 2016, **394**, 176-184.
41. F. Yang, S. Zhang, D. Yang and X. Jian, *Journal of Membrane Science*, 2007, **301**, 85-92.
42. S. Wang, J. Cai, W. Ding, Z. Xu and Z. Wang, *Membranes*, 2015, **5**, 369-384.
43. T. H. Lee, M. Y. Lee, H. D. Lee, J. S. R. Hyo, W. K. Ho and B. Park, *Journal of Membrane Science*, 2017, **539**, 441-450.
44. J. R. Werber, C. J. Porter and M. Elimelech, *Environ. Sci. Technol.*, 2018, **52**, 10737-10747.
45. W. Yuan and A. L. Zydney, *Environ. Sci. Technol.*, 2000, **34**, 5043-5050.

46. Y. L. Lin, P. C. Chiang and E. E. Chang, *J. Hazardous Mat. B*, 2006, **137**, 324-331.
47. J. Lowe and M. M. Hossain, *Desalination*, 2008, **218**, 343-354.
48. Q. Saren, W. Rong, G. Chaitra, J. Torres, X. Hu and A. G. Fane, *Journal of Membrane Science*, 2016, **508**, 94-103.
49. W. Ding, J. Cai, Z. Yu, Q. Wang, Z. Xu, Z. Wang and C. Gao, *J. Mater. Chem. A*, 2015, **3**, 20118.

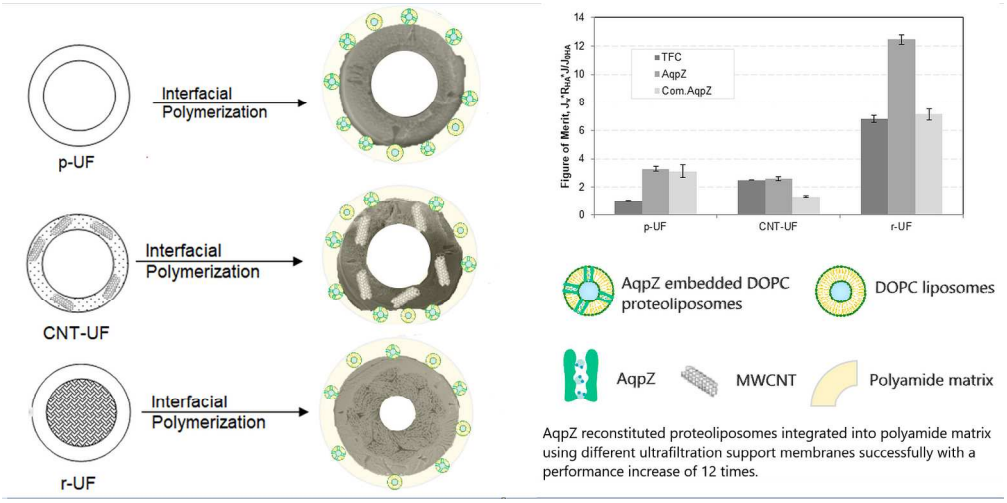

671x331mm (96 x 96 DPI)